

Rotating white dwarf models with finite-temperature envelope

Shin'ichirou Yoshida [★]

¹ *Department of Earth Science and Astronomy, Graduate School of Arts and Sciences, The University of Tokyo, Komaba 3-8-1, Meguro-ku, Tokyo 153-8902, Japan*

ABSTRACT

We present new numerical method to compute structures of differentially rotating white dwarfs with thermal stratification. Our models have cores composed of ions and completely degenerate electrons and have isentropic envelopes composed of ions, photons, partially degenerate electrons and positrons. The models are intended to mimic very early phases of remnants of white dwarf binary mergers, some of which may lead to type Ia supernovae. The effect of hot envelope to increase the mass depends on its chemical composition through the mean molecular weight of the envelope. For uniformly rotating models, we see only a small increase in mass even in the presence of hot envelope. Differential rotation changes it drastically and super-Chandrasekhar mass model whose mass doubles the Chandrasekhar mass of the degenerate star for some parameter choices. We also compute quasi-equilibrium evolutionary sequences of remnants by fixing either total angular momentum or entropy in the envelope. Existence of these sequences depends on various factors such as the remnant mass, the profile of differential rotation, the entropy and the chemical composition of the envelope.

Key words: white dwarfs – stars: rotation

1 INTRODUCTION

Mergers of two white dwarfs in binary systems driven by gravitational wave emission are almost certain to be detected by the planned space-borne laser interferometers such as European-American eLISA (Evans et al. 1987; Nelemans 2009), Chinese TianQin (Luo et al. 2016), and Japanese DECIGO (Kawamura et al. 2006). The most interesting possibility after mergers is that a sufficiently massive merger remnant may lead to type Ia supernovae (SNeIa), whose total mass exceeds the Chandrasekhar mass of white dwarfs (Webbink 1984; Iben & Tutukov 1984). On the contrary there have been also claims against the successes of this channel to SNeIa, producing neutron stars instead (Saio & Nomoto 1985; Nomoto & Kondo 1991).

For smaller mass binaries where SNeIa do not occur, former studies have presented discussions and evidences that subdwarf O stars, R-Corona Borealis stars, and carbon stars may be formed through their mergers (Webbink 1984; Clayton et al. 2007; Izzard et al. 2007; Longland et al. 2011). Another interesting possibility is that a white dwarfs with strong magnetic field of $10^6 - 10^9$ G may be created as a remnant of the mergers (Wickramasinghe & Ferrario 2000; García-Berro et al. 2012). It is also intriguing a bimodal

distribution in white dwarf mass revealed by *Gaia* Data Release 2 may point to the possibility that some if not all of the massive white dwarfs are formed through the mergers (Kilic et al. 2018).

Considering the richness of binaries and white dwarfs in the Universe, we expect these merging events are not at all rare. For instance, Rueda et al. (2018) estimates the overall cosmic merger rate of white dwarf binaries as $(3.7 - 6.7) \times 10^5 \text{Gpc}^{-3} \text{yr}^{-1}$ by using an event rate per mass (Maoz et al. 2018) and an extrapolated number of galaxies (Kalogera et al. 2001).

In common merger of a binary with a low mass degenerate member having a larger radius it is disrupted by unstable Roche-lobe overflow or tidally disrupted to accrete onto a more massive star. The massive member becomes a core of the remnant whose temperature does not rise initially and is nearly degenerated. On top of it the debris of lighter star forms a thick and hot envelope, which is heated up by direct impact or accretion shock. The remnant just after the merger rotates rapidly with strong degree of differential rotation. As a result the remnant is highly flattened by the centrifugal force. After the merger, the remnant object evolves through viscous and thermal relaxation. There have been precedent works mainly focused on these long time evolution processes (Yoon et al. 2007; Shen et al. 2012; Schwab et al. 2012, 2016). Shen et al.

[★] E-mail: yoshida@ea.c.u-tokyo.ac.jp

(2012) characterizes the early phase of remnant evolution in three stages. After a few dynamical timescale of a remnant (a few second, assuming a normal white dwarf), it settles to a (quasi-)hydrostationary state. Then in 10^4 to 10^8 s, the remnant gradually adjusts its differential rotation to a uniform one through the action of viscosity. The timescale may depend on the so-called α parameter of turbulent viscosity, thus may be regulated by the magneto-rotational instability (Balbus & Hawley 1991) and/or viscous boundary layer at the boundary between the core and the envelope. After 10^3 to 10^4 yrs, the thermal relaxation proceeds in which the Kelvin-Helmholtz contraction of the envelope takes place and substantial heat is transported to the core.

In this paper we focus on the modeling of the quasi-hydrostationary state of the remnants before the viscosity smooth out the initial differential rotation. As the thermal relaxation of the objects is expected to come later, an object is modeled with two different thermal layers, i.e., the cold core and the hot envelope. This phase of the remnants lasts for a rather short period, only 10^4 s at most (Shen et al. 2012). It is, however, interesting to consider remnants in this phase with short duration since the dynamical processes in and stability of massive remnants may be a clue to a prompt explosion of SNeIa (Kashyap et al. 2017).

2 FORMULATION

2.1 Assumptions on the model

A star we have in mind is a merger remnant of two white dwarfs. According to numerical hydrodynamics simulations of white dwarf mergers (Benz et al. 1990; Segretain et al. 1997; Lorén-Aguilar et al. 2005, 2009; Yoon et al. 2007; Dan et al. 2011, 2012, 2014; Pakmor et al. 2012; Raskin et al. 2012; Tanikawa et al. 2015; Sato et al. 2015, 2016), a low mass member of the binary having a larger radius is disrupted and accretes onto a more massive primary star. The accreted matter from the secondary is initially heated up by liberating its gravitational binding energy and forms an extended envelope around the primary. The temperature of the gas may be as high as 10^9 K (Yoon et al. 2007) in the envelope and is partially degenerate. The initial temperature range of the remnant may also be estimated by assuming the mechanical energy of the binary at the onset of the Roche-lobe filling of the secondary goes to the internal energy of the formed envelope. This estimate gives the same order of the temperature in the envelope. On the other hand the core remains cold and degenerate until significant thermal conduction occurs. The timescale may be 10^3 yrs (Shen et al. 2012), thus we neglect the heating of the core. Initially the merger remnant is rapidly rotating with high degree of differential rotation and the viscosity let the rotational profile evolve to that of uniform rotation in 10^4 to 10^8 s. We are interested in these initially differentially rotating remnants which lasts much shorter timescale than that of the thermal evolution. The rotational profile has a nearly uniformly rotating core with a differentially rotating envelope (see e.g., Fig.6 in Yoon et al. (2007) ; Fig.1 in Schwab et al. (2012) ; Fig.1 in Shen et al. (2012)). As for the envelope, we assume it isentropic for simplicity. The hot envelope with temperature of 10^9 K radiatively cools down. They tend to develop

convection (Loeb & Rasio 1994) which leads to the nearly isentropic (neutrally stable to convection) thermal structure (Kippenhahn & Weigert 1994). Some of the hydrodynamic simulations of white dwarf mergers also supports this simplification, in which entropy profile is nearly flat in the outer region of the remnants except at their surface (see Fig.1 in Zhu et al. (2013), and Figs.2 and 7 in Schwab et al. (2012))

2.2 Equation of state of degenerate core

As the equation of state (EOS) of completely degenerate core, we use the analytic expression of pressure and density as a function of dimensionless Fermi momentum x (Shapiro & Teukolsky 1986). It should be noted that the correction due to ion Coulomb interactions are important in realistic white dwarfs (e.g. Sec.2.4 of Shapiro & Teukolsky (1986)). We neglect the correction in this paper for simplicity. Mass density ρ and pressure p are related as

$$\rho = bx^3 \quad (1)$$

$$p = a \left(x(2x^2 - 3)(x^2 + 1)^{1/2} + 3 \ln \left(x + \sqrt{1 + x^2} \right) \right). \quad (2)$$

Here x is the dimensionless Fermi momentum of electron, $x = p_F/m_e c$ where p_F is the Fermi momentum, m_e is the mass of electron and c is the speed of light. The value of a and b are

$$a = 6.00 \times 10^{22} \text{ dyn/cm}^2 \quad (3)$$

$$b = 9.82 \times 10^5 \mu_e \text{ g cm}^{-3}, \quad (4)$$

where μ_e is mean molecular weight of electron. Enthalpy h is given by

$$h = \frac{8a}{b} \sqrt{1 + x^2}. \quad (5)$$

2.3 Equation of state of hot envelope matter

For the EOS of hot envelope matter, we adopt the so-called 'Helmholtz' EOS by Timmes & Swesty (2000).¹ The EOS assumes the gas is composed of several species of ions, photons, electrons and positrons. The electrons and positrons have arbitrary degrees of degeneracy and relativity. The numerical EOS is constructed by forcing the thermodynamical consistency when interpolating Helmholtz's free energy. Given mass density, temperature, mass fraction of ion species, the original subroutine computes various thermodynamical quantities such as pressure, entropy, internal energy density, sound speed, and adiabatic exponents. Whenever other combination of thermodynamical variables are needed as input values, we develop wrapper routines that iteratively solve for the variables by calling the original subroutine.

2.4 Basic equations of hydrostationary configurations

Basic equations of hydrodynamics assuming stationary and axisymmetric equilibrium are the momentum equation

$$-\frac{1}{\rho} \nabla p - \nabla \Phi - R \Omega(R)^2 = 0, \quad (6)$$

¹ We use the Fortran subroutine codes and data tables provided at http://cococubed.asu.edu/code_pages/eos.shtml.

and the Poisson equation for gravitational potential,

$$\Delta\Phi = 4\pi G\rho. \quad (7)$$

Ω is the rotational angular frequency of the star which is a function of cylindrical radius R defined as $R = r \sin\theta$ where r and θ are the spherical polar coordinate whose origin is that of the star. We neglect the effect of general relativistic gravity in our models, which may significantly affect the result for very massive stars (Boshkayev et al. 2011, 2014; Mathew & Nandy 2017; Carvalho et al. 2018). In a domain of a star in which fluid is regarded as barotropic (i.e., density depends only on pressure), Poincarè-Wavre theorem (Tassoul 1978) tells us that the rotational angular frequency depends only on the distance from the rotational axis. Since our stellar models have a degenerate core (zero entropy core) and an isentropic envelope, the angular frequency satisfies the condition of the theorem. We further assume that the angular frequency distribution is continuous at the core-envelope boundary for simplicity.

In this paper physical quantities are normalized as follows (variables with tilde are dimensionless).

$$\frac{\rho}{\rho_c} = \tilde{\rho} \quad (8)$$

$$\frac{p}{p_c} = \tilde{p} \quad (9)$$

$$\frac{\Omega}{\sqrt{4\pi G\rho_c}} = \tilde{\Omega} \quad (10)$$

$$\frac{r}{R_\star} = \tilde{r} \quad (11)$$

$$\frac{\Phi}{R_\star^2 4\pi G\rho_c} = \tilde{\Phi} \quad (12)$$

Here R_\star is the equatorial surface radius, ρ_c is density at the origin and p_c is pressure at the origin. With this normalization we introduce dimensionless parameter β in the theory

$$\beta = \frac{p_c}{4\pi G\rho_c^2 R_\star^2}. \quad (13)$$

Dimensionless enthalpy is defined as

$$\tilde{h} := \int \frac{d\tilde{p}}{\tilde{\rho}}. \quad (14)$$

Note that a term in the equation containing dimensional enthalpy should be multiplied by β . In the following we omit tilde from dimensionless quantities. The momentum equation Eq.(6) is integrated to result in

$$\beta h + \Phi - \int_0^R u\Omega(u)^2 du = C, \quad (15)$$

where C is a constant of the first integral (normalized by $4\pi G\rho_c^2 R_\star^2$) of the momentum equation. Notice that Ω is a function of $u = r \sin\theta$. Different values of the constant C are assigned to each domain of isentropy. The Poisson's equation is cast into an integral equation by using an appropriate Green's function $G(\vec{r}, \vec{r}')$,

$$\Phi(\vec{r}) = \int G(\vec{r}, \vec{r}')\rho(\vec{r}')dV', \quad G(\vec{r}, \vec{r}') \equiv -\frac{1}{4\pi|\vec{r}' - \vec{r}|}. \quad (16)$$

2.5 Rotation laws

For differentially rotating barotropic-star models, different analytic forms of rotational profile (i.e., functional forms of

angular frequency) are proposed in the literatures (see e.g., Eriguchi & Müller (1985); Hachisu (1986a)).

We present results of three representative rotational profiles compatible with barotropic fluid. In all cases we introduce dimensionless parameter k_0 by which the last term in the left hand side of Eq.(15) is written as

$$\int_0^R \Omega(u)^2 u du \equiv k_0 \Psi(R). \quad (17)$$

The constants in Ψ for each case is chosen in such a way that $\Psi(R=0) = 0$.

2.5.1 Uniform rotation

In this case we define $k_0 = \Omega_0^2$ as a constant which amounts to the rotational frequency on the symmetry axis (and throughout the fluid). Ψ is given as,

$$\Psi = \frac{1}{2}R^2. \quad (18)$$

2.5.2 Slowly rotating core remnants – "Yoon07"

Yoon et al. (2007) investigates a secular evolution of a remnant of carbon-oxygen white dwarf merger. Their initial model of the remnant consists of slowly and uniformly rotating core and a rapidly and differentially rotating envelope. Figure 6 of Yoon et al. (2007) gives the angular frequency profile of the remnant. The profile is well-approximated with a simple function,

$$\Omega = \begin{cases} \sqrt{k_0} & (R \leq r_b) \\ \sqrt{k_0} \frac{r_b^3}{\epsilon_b^{5/4}} R^{-3} (R-b)^{5/4} & (R \geq r_b), \end{cases} \quad (19)$$

where r_b is the equatorial core radius, ϵ_b is a small parameter making the angular velocity Ω continuous at r_b , and $b \equiv r_b - \epsilon_b$ (Fig.1). We name the rotation law "Yoon07". The integral Ψ is written as

$$\Psi = \begin{cases} \frac{k_0}{2} R^2 & (R \leq r_b) \\ k_0 \left(F(R) - F(r_b) + \frac{r_b^2}{2} \right) & (R \geq r_b) \end{cases} \quad (20)$$

where $F(R) \equiv \frac{5 \tan^{-1}\left(\frac{\sqrt{R-b}}{\sqrt{b}}\right)}{64b^{3/2}} + \frac{\sqrt{R-b}(-48b^3+136b^2R-118bR^2+15R^3)}{192bR^4}$. The uniformly rotating core, formerly being a primary star, is slowly rotating while the envelope has a large angular momentum inherited from the orbital angular momentum of the secondary. Outside the core, there is a small region where the angular frequency increases as a function of R . Ω in the outer envelope monotonically decreases.

2.5.3 Fastly rotating core remnants – "Kepler"

A rotation law that resembles that of Keplerian flow ($\Omega \sim R^{-3/2}$) in the envelope may be defined as

$$\Omega = \frac{\sqrt{k_0}}{R^{3/2} + D^{3/2}}, \quad (21)$$

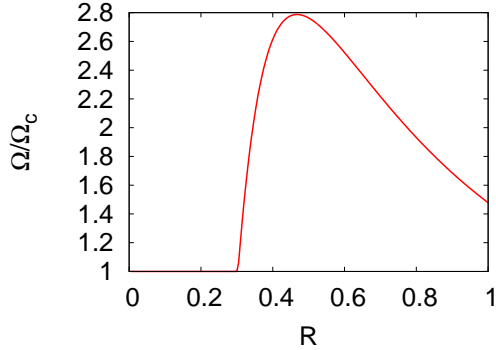


Figure 1. A characteristic profile of angular frequency profile of a star with a slowly rotating core (Eq.(19)). The distance from the rotational axis is normalized by the equatorial radius of the star and the angular frequency is normalized by the that of the uniformly rotating core. In this normalization $r_b = 0.3$ and $\epsilon_b = 3 \times 10^{-2}$ for this example.

that gives $\Psi = \psi(R) - \psi(0)$, where

$$\psi = \frac{1}{9} \left(-\frac{6\sqrt{R}}{D^{3/2} + R^{3/2}} - \frac{2\sqrt{3} \tan^{-1} \left(\frac{1 - \frac{2\sqrt{R}}{\sqrt{D}}}{\sqrt{3}} \right)}{D} + \frac{\ln \frac{(\sqrt{D} + \sqrt{R})^2}{D^2 - DR + R^2}}{D} \right) \quad (22)$$

We hereafter call this rotation law "Kepler". For $R \ll D$, the profile limits to that of the uniform rotation. In the other extreme, $R \gg D$, $\Omega \sim R^{-3/2}$. In general D is not necessarily the radius of the core r_b , but we set $D = r_b$, which means the rotational profile change its slope at r_b . In this rotational profile the core is rotating more rapidly than the envelope whose rotational profile asymptotes to the Keplerian. This profile is motivated by the result of a merger simulation by Shen et al. (2012) (see their Figs.1 and 3) in which the accreted matter from the secondary forms a hot Keplerian disk around the primary. Apart from the narrow transition region, the core rotates faster than the Keplerian envelope in their result. Although the profile is different from that of Yoon et al. (2007), we explore this possibility as well.

2.6 Our self-consistent field method

Hachisu (1986b,c) presented a versatile method (Hachisu's self-consistent field (SCF) method, HSCF method) of solving stellar equilibrium configurations that stably solves highly deformed equilibrium configuration of a single star or binary stars. The method gives convergence to rapidly and differentially rotating stellar models close to mass-shedding limit for general barotropic equation of state with various stiffness. By using HSCF Hayashi et al. (1998) studied differentially rotating hot cores of massive stars ("fizzlers") in which they took into account finite temperature effect. They fix en-

tropy and electron fraction so that the EOS is mimicked by a barotropic one. Fujisawa (2015) developed an extension of the HSCF to finite temperature and non-barotropic stars by assuming shellular rotation law in which angular frequency is an analytic function of radial coordinate. The method improved a formerly-developed numerical method that directly solves a discretized set of partial differential equations by using Newton-Raphson scheme (Uryu & Eriguchi 1994, 1995).

Here we present a new SCF formalism to compute rapidly rotating multi-temperature stellar model based on the assumptions in the previous sections. Our stellar model consists of two zones each of which is barotropic (zero entropy in the core and isentropic in the envelope). Thus there appear two constants of Eq.(15), which we name C_{in} and C_{out} . C_{in} is for the degenerate core and C_{out} is for the hot envelope. Other parameters to be fixed are β and k_0 .

The schematic configuration of the star is shown in Fig.2. Point 'O' is the origin, at which star's center of mass resides. Point 'A' is at the equatorial surface of the star. Point 'P' is an intersection of the symmetric axis of the star with the surface. 'B' is a point on the core-envelope boundary on the equatorial plane. Our SCF type iterations are done as follows (procedure [a] to [h]).

[a] First the model parameter is provided. They are the central density (ρ_c), the ratio of the pressure at B to the central pressure (f_p), the envelope temperature at B (T_b), the polar and equatorial axis ratio ($a_x \equiv \overline{OP}/\overline{OA}$), the chemical composition of the core and the envelope. Notice that the point B is not initially specified, but f_p is.

[b] The function Ψ of rotational integral (Eq.17) is computed on the grid points.

[c] Enthalpy distribution on the computational grid points is initially guessed.

[d] At each grid point density is computed through the EOS routines.

[e] The density distribution is plugged into Eq.(16) to compute the gravitational potential Φ .

[f] The distance r_b between O and B, β , k_0 , C_{in} , C_{out} are iteratively solved. The five equations solved are, Eq.(15) evaluated at O, A, P, and at B for $r = r_b - 0$ (core), as well as the continuity of pressure at B, i.e., $p(r_b - 0, \pi/2) = p(r_b + 0, \pi/2) \equiv p_b$. The boundary between the core and the envelope is specified by the ratio f_p . We use Newton-Raphson method to solve for these parameters.

[g] Once the parameters above are fixed, we compute the enthalpy at each grid points by Eq.(15). The surface of the star is identified as zeroes of pressure.

[h] If the residual of enthalpy from that of the former iteration is small enough, we have a solution. Otherwise we continue the iterations.

The quality of a converged solution is measured by the virial check (Hachisu 1986b), VC ,

$$VC \equiv \left| 2 \int \rho(R\Omega)^2 dV + \int \rho\Phi dV + 6\beta \int p dV \right|. \quad (23)$$

For grid numbers of $(r, \theta) = (200, 50)$ we have $VC = \mathcal{O}[10^{-3}]$, compared to $\mathcal{O}[10^{-4}]$ for the original HSCF. The slightly degraded quality of the current method reflect the discontinuity of such thermodynamic variables as ρ at the core-envelope boundary. Though pressure is made continuous

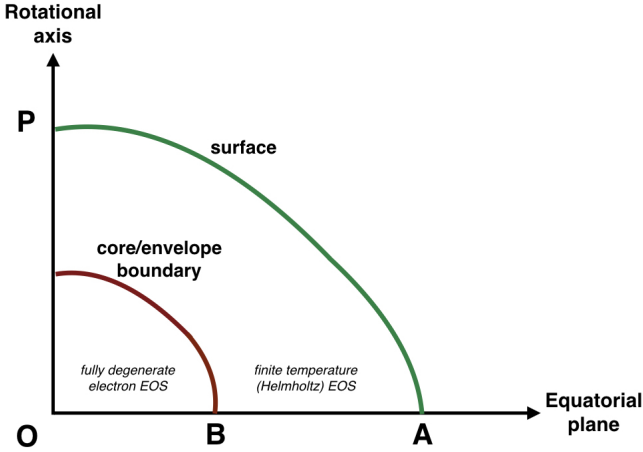


Figure 2. Schematic figure of the quadrant of the meridional section of the star. We assume the star is axisymmetric as well as symmetric with respect to its equatorial plane. Point 'O' is the origin, at which star's center of mass resides. Point 'A' is at the equatorial surface of the star. Point 'P' is an intersection of the symmetric axis of the star with the surface. Point 'B' is a point on the core-envelope boundary on the equatorial plane.

there, density is discontinuous because of the temperature and entropy discontinuity.

How fast a star is rotating is characterized by different parameters which are appropriate in different contexts. One of the most frequently used parameter is so-called 'T/W' value (Tassoul 1978) which is defined by the ratio of rotational kinetic energy to gravitational energy as

$$T/W \equiv \frac{\frac{1}{2} \int \rho R^2 \Omega^2 dV}{\frac{1}{2} \left| \int \rho \Phi dV \right|}. \quad (24)$$

The global parameter is conventionally used to characterize how fast the star is rotating even when the star is highly differentially rotating. It should be noted that the large degree of differential rotation does not necessarily mean large value of T/W .

We have several parameters to be fixed to compute a model star, which are listed in Table.1 Apart from these we also need the parameters to specify the law and degree of differential rotations (sec.2.5) when computing a differentially rotating star. Physical significance of some of these parameters is worth mentioning. In our models the core-envelope boundary is characterized by the relative value of pressure to the central value, f_p . It determines the position of the cut-off of the core beyond which the EOS is switched to that of the finite temperature. Therefore, together with ρ_c it determines the core mass and radius. Temperature at the core-envelope boundary, T_b , together with ρ_c and f_p fixes the entropy of the envelope, which determines the mass and the radius of the envelope. T_b does not affect the core characteristics. A large value of f_p may result in a smaller mass of the core than that of the envelope, which is not natural for a merger remnant model. On the other hand very small f_p results in a model which is similar to the completely degenerate model. In this paper, we adopt the range of f_p with $\mathcal{O}[f_p] \sim 0.01-0.1$

ρ_c	central mass density
$p_b/p_c \equiv f_p$	dimensionless pressure at the core-envelope boundary
T_b	temperature at the core-envelope boundary
$(Z/A)_c$	ratio of atomic to baryon number in the core
X_H	hydrogen fraction in the envelope
X_{He}	helium fraction in the envelope
X_C	carbon fraction in the envelope
X_O	oxygen fraction in the envelope
r_p/r_e	axis ratio

Table 1. Parameters to be fixed to compute our models Apart from these parameters we also need to fix the parameters to specify the rotation law in Sec.2.5 when dealing with a differentially rotating star.

so that the models have a sufficiently large core mass but the envelope is also important.

It should be remarked that Kadam et al. (2016) extended the HSCF scheme to handle two layers of polytropic gas. Our formulation is different from theirs in the following points. Firstly we have the EOS of degenerate electrons in the core and the tabulated finite-temperature EOS in the envelope, while Kadam et al. (2016) assumes polytropic EOS. Secondly we allow different temperature at the core-envelope boundary. Thirdly we allow the stars to have differential rotation, rather than assuming uniform rotation. All these features in our formulation are motivated by the merger remnant of white dwarf binaries.

3 RESULTS

In this paper we assume for simplicity that the core is made of elements whose ratio of mass to atomic number is 2. This roughly applies to helium, carbon, oxygen, and neon, For magnesium the ratio is 2.03, which is still well approximate by 2. The simple EOS of completely degenerate electrons is characterized by the mean molecular weight per electron $\mu_e = Y_e^{-1}$, where Y_e is the electron fraction. Our core model does not distinguish the difference among heavy elements.

Following Boshkayev & Quevedo (2018) we take the central density of the core to be $\rho_c < 1.37 \times 10^{11} \text{gcm}^{-3}$, beyond which the inverse β reaction destabilizes the core.²

As for the numerical mesh, we use uniformly-separated grid points in r, θ direction of the spherical polar coordinate. Since our models are supposed to have the equatorial symmetry, we restrict θ as $0 \leq \theta \leq \pi/2$. All of the models in the paper are computed with the radial grid number, $N_r = 200$ and the angular grid number $N_\theta = 100$. Doubling each of the grid numbers results in the residual of order $10^{-2}\%$ in the total mass for rapidly rotating (axis ratio = 0.5) models with differential rotation. The residuals in gravitational, kinetic

² It should be noted that this choice may overestimate the maximum density possible. Maximum central density of a white dwarf with a typical composition may be less than 10^{10}gcm^{-3} , beyond which pycnonuclear reaction of carbon occurs in an C-O white dwarf, while pycnonuclear (Gasques et al. 2005) and electron captures on ^{20}Ne occurs in an O-Ne star (Miyaji et al. 1980). I thank the anonymous referee for pointing these out and suggesting the appropriate references.

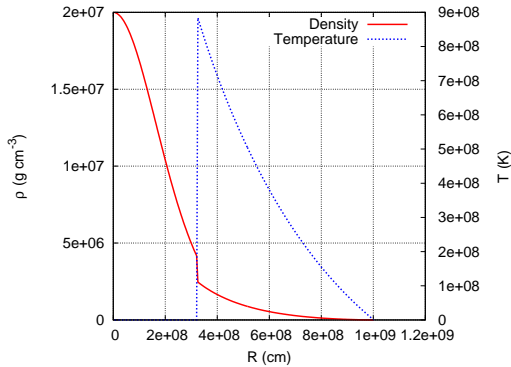


Figure 3. Density and temperature distribution of a typical equilibrium state. The central density is $\rho_c = 2 \times 10^7 \text{ g cm}^{-3}$ and the temperature at the core-envelope boundary is $T_b = 9 \times 10^8 \text{ K}$. The relative pressure at the core-envelope boundary and at the center is $f_p = 10^{-1}$. It should be noted that due to the finite number of grid points, the largest temperature shown in the plot seems less than T_b , which is an artifact of the plot.

and thermal energy are of the same order. The residual of core mass is larger but at most 1%.

3.1 Non-rotating stars

First we see the effect of finite temperature envelope on the global structure of a star in the non-rotating limit. In Fig.3 a typical density and temperature profile is shown as a function of radial coordinate. The density and the temperature is discontinuous at the core radius $R_c = 3.2 \times 10^8 \text{ cm}$, though the pressure is made continuous there (sec.2.6).

In Fig.4 mass-radius relation of non-rotating stars are plotted. Chemical composition of the envelope are $X_C = 0.2$ and $X_O = 0.8$ in the mass fraction. On each curve we change the central density of the core while fixing the pressure ratio f_p which specifies the boundary between the core and the envelope, and the temperature T_b there. For comparison we plot the mass-radius of completely degenerate stars. We see the following characteristics of the equilibria. Firstly, as we increase the central density the core starts to dominate the envelope and the stellar structure tends to resemble to that of white dwarfs supported by completely degenerate electrons. Deviation from the degenerate model is seen in the low central density models for sufficiently high temperature of the envelope. Comparing $f_p = 2 \times 10^{-2}$ models, we see the lower temperature ($T_b = 10^8 \text{ K}$) sequence is almost on top of the degenerate sequence, while the higher temperature sequence has the larger radius than the degenerate star with the same mass. As the central density decreases, the core mass decreases while its radius increases. The surface gravity of the core is reduced and the hot envelope expands rapidly as a function of ρ_c . The mass fraction of the envelope increases and the total mass starts to increase again as the central density decreases. The increasing envelope mass is supported by the thermal gas pressure of the hot gas.

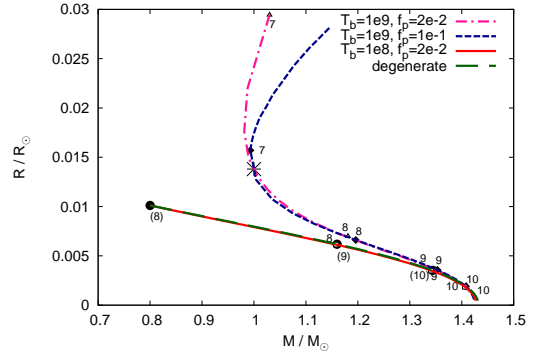


Figure 4. Mass-radius relations of non-rotating stars. Mass fraction of elements are $X_C = 0.2$ and $X_O = 0.8$. On each curve, the pressure ratio f_p and the temperature at the core-envelope boundary T_b are fixed. The numbers attached to the curves are $\log_{10}[\rho_c/1 \text{ g cm}^{-3}]$. The curve labeled as 'degenerate' is the mass-radius relation of the star with the same composition. The asterisk on the sequence with $T_b = 10^9 \text{ K}$ and $f_p = 10^{-1}$ marks the point below whose central density the star has a larger mass in the envelope than in the core. Notice that the sequence with $T_b = 10^8 \text{ K}$ and $f_p = 2 \times 10^{-2}$ is almost on top of the completely degenerate one.

By increasing the fractional pressure f_p at the core-envelope boundary, we have an enhanced effect of hot envelope. Since f_p parametrize the cut-off of the core region, a smaller value means the core region has a larger fraction in the star. As a result when f_p decreases, the mass-radius relation of the core asymptotes to that of fully degenerate stars. The envelope, on the other hand, has a larger entropy and swells up so that the stellar radius grows, although the mass of the envelope do not contribute to the total mass so much. When f_p increases, the core mass is reduced and the stellar structure becomes relatively envelope-dominated. In this case, the envelope can sustain a larger mass than that of the fully degenerate star.

It should be noted, however, that the models whose envelope mass is larger than that of the core would not be realized in binary merger events, since the less massive secondary star in a binary has a larger radius and is disrupted tidally to accrete onto the more massive primary to form a hot envelope. On the sequence with $T_b = 10^9 \text{ K}$ and $f_p = 10^{-1}$, the branch above the 'asterisk' has a larger mass in the envelope than in the core.

We show in Fig.5 the dependence of the mass-radius relation on the envelope's chemical composition. We compare the cases that have different fraction of (X_H, X_{He}, X_C, X_O) in the envelope. Filled circles mark the points above which the envelope mass exceeds that of the core. On dashed curves the envelope mass always exceeds that of the core. We notice that the difference in the fraction of the hydrogen in the envelope affects the relation more than the difference in the other elements. As we increase the hydrogen fraction more massive models are allowed. On the other hand the models with no hydrogen in the envelope differ slightly each other.

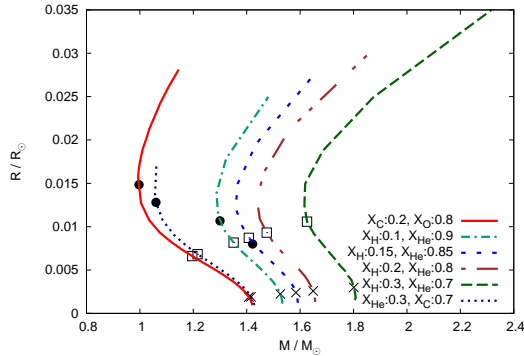


Figure 5. Mass radius relations for models with different compositions in the envelope. We fix $T_b = 10^9$ K and $f_p = 10^{-1}$. The range of the central density on these sequence is $10^7 \leq \rho_c / 1\text{g cm}^{-3} \leq 10^{11}$. A filled circle marks the point above which the envelope mass exceeds that of the core (envelope dominant). The open squares and crosses mark the models whose central density are 10^8g cm^{-3} and 10^{10}g cm^{-3} respectively. Dashed curves are always envelope dominant.

This feature is understood as originating from the difference in the mean molecular weight. For gas with fixed density and temperature, as the mean molecular weight decreases the pressure increases. The mean molecular weight decreases as we increase the hydrogen fraction, while it does not change as for the other elements. Thus the part of the thermal pressure supporting the envelope mass and radius rises as the hydrogen fraction increases. Consequently higher mass model is realized for the same central density and the temperature of the core-envelope boundary when we increase the hydrogen fraction.

3.2 Uniformly rotating stars

Next we summarize the characteristics of uniformly rotating stars.

Our modified HSCF code can compute a sequence of rotating stars up to the mass-shedding limit at which the matter at the equatorial surface is in the state of balance between centrifugal and gravitational force. The enthalpy gradient does not contribute to the mechanical balance at the limit. With a faster rotation the matter would be shed from the surface of the star, thus the equilibrium sequence terminates at the limit.

In Fig.6 logarithm of the pressure is shown as a contour plot. The model is slightly below the mass shedding limit with $T/W = 1.78 \times 10^{-2}$. The highly flattened stellar configuration due to the centrifugal force is apparent.

In Fig.7 we plot the mass-radius relation of a uniformly rotating star's equilibrium sequence up to its mass-shedding limit. All the models have the fixed temperature at the core-envelope boundary $T_b = 5 \times 10^8$ K and the composition both in the core and the envelope $(X_C, X_O) = (0.2, 0.8)$. To construct each sequence we additionally fix ρ_c and f_p . For uniformly

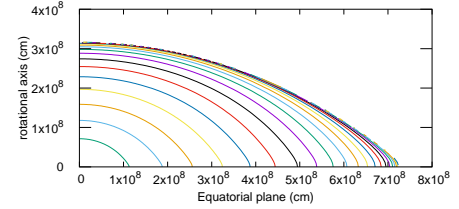


Figure 6. Pressure contour of a uniformly rotating star close to its mass-shedding limit. Thirty levels surfaces are equally spaced in logarithm of pressure. Assuming the axial and equatorial symmetry, we only plot a quadrant of the meridional cross section. The central density is 10^8g cm^{-3} , pressure at the core-envelope boundary is $f_p = 10^{-1}$ and temperature at the boundary is $T_b = 5 \times 10^8$ K. The total mass of the star is $1.37M_\odot$, while the core mass is $0.719M_\odot$. The equatorial core radius is 2.09×10^8 cm. Dimensionless parameter $T/W = 2.61 \times 10^{-2}$, which corresponds to rotational angular frequency $\Omega = 0.687$ Hz.

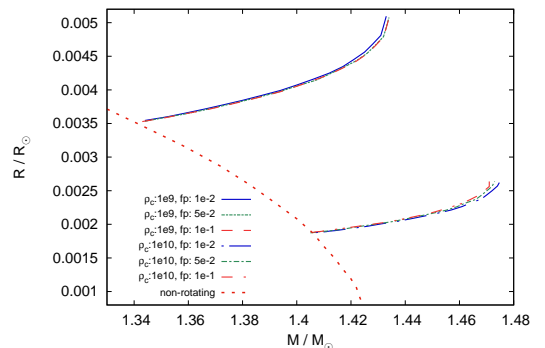


Figure 7. Mass-radius relation of uniformly rotating model sequence in the envelope. The rightmost point of each curve corresponds to the mass-shedding limit. The curve labeled as "non-rotating" is the mass-radius curve for the non-rotating model.

rotating stars, both the total and the core mass increase at most by a few percent even at the mass-shedding limit. The core radius increases by a few percent while the radius of the envelope increases by tens of percent. For a uniformly rotating star to have a large mass, it needs to have large T/W so that the rotational contribution to the force balance of the stellar fluid becomes significant. When the stellar EOS is soft (i.e. the adiabatic index is small), the rotational sequence of equilibrium reaches the mass-shedding limit before T/W reaches such a large value that the mass increases significantly. The volume-averaged adiabatic index of the en-

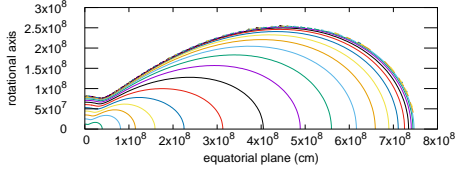


Figure 8. Pressure contour of a differentially rotating star with Yoon07 profile close to its mass-shedding limit. Thrity levels surfaces are equally spaced in logarithm of pressure. The central density is 10^8 g cm^{-3} , pressure at the core-envelope boundary is $f_p = 10^{-1}$ and temperature at the boundary is $T_b = 5 \times 10^8 \text{ K}$. The total mass of the star is $2.31M_\odot$, while the core mass is $0.785M_\odot$. The equatorial core radius is $1.01 \times 10^8 \text{ cm}$. Dimensionless parameter T/W amounts to 6.20×10^{-2} and the rotational angular frequency $\Omega = 0.852 \text{ Hz}$ at its equatorial surface. Pressure maxima is at the coordinate origin.

velope is about 1.6, which is too soft to support a large increase in mass compared to the non-rotating model. As is seen in Fig.7 the mass-radius relation is scarcely changed by changing the pressure fraction f_p .

3.3 Differentially rotating stars: Yoon07 rotation law

As the first examples of differentially rotating models, we consider stars whose rotational profile is that of Sec.2.5.2. We hereafter call it Yoon07 rotation law.

The rotation law allows much larger value of angular momentum and T/W for given ρ_c, f_p, T_b than the corresponding models with uniform rotation. In Fig.8 we show an isocontour plot of pressure for a typical model of nearly mass-shedding limit that is to be compared with Fig.6. The star has a small core whose equatorial radius is roughly 1/7 of the envelope radius. The configuration is highly flattened due to the centrifugal force, with a small flattened core surrounded by a massive disk-like envelope.

Mass-Radius relations (Fig.9) show that a differentially rotating sequence may reach larger mass and radius models than the uniformly rotating counterpart. For given ρ_c and T_b , larger f_p leads to larger increments in mass and radius compared with the uniformly rotating model seen in Fig.7. This is because a larger f_p means the cold degenerate core is truncated at a smaller mass and the hot envelope is attached to it with the larger pressure. It corresponds to a smaller contribution to the entire star from the core which rotates slowly. The hot envelope may be rapidly rotating in this rotation law to sustain a large mass and to be extended to a large radius.

A qualitatively different behaviour of sequences for different f_p is noticed in Fig.9. For instance, the sequences with $f_p = 10^{-1}$ and 5×10^{-2} show monotonic increase in radius and mass as the star spins up, while the sequence with $f_p = 10^{-2}$ shows non-monotonic change in mass. The difference origi-

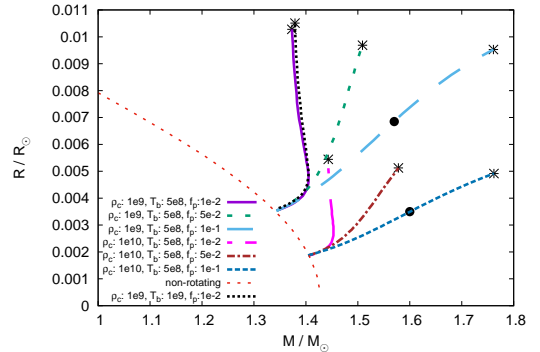


Figure 9. Mass and radius of the Yoon07 rotation law for different values of f_p . We fix the chemical composition of both in the core and in the envelope as $(X_C, X_O) = (0.2, 0.8)$. Filled circles mark the points above which the envelope mass exceeds that the core. The asterisks show the mass-shedding limit of the sequences.

nates from our parametrization to construct the sequences. As for the parameter to quantify the rotational deformation of a star we use the axis ratio which is the ratio between the polar and the equatorial radii of the star. For a star with sufficient mass contribution from its envelope whose f_p value is large, the deformation quantified by the axis ratio monotonically corresponds to other characteristics of measuring stellar rotation rate such as angular momentum or T/W parameter. In Fig.10 (a) the angular momentum for $f_p = 10^{-1}$ case is plotted as a function of the axis ratio. It should be noted for non-rotating stars the axis ratio is unity. The angular momentum increases as the stellar deformation by rotation is enhanced. Therefore the parametrization by the axis ratio is faithful to the rapidness of rotation measured by the angular momentum. For $f_p = 10^{-2}$ case (panel (b)), however, the angular momentum is not a monotonic function of the axis ratio. Thus the sequence is not regarded as that of increasing degree of rotation.

3.4 Differentially rotating stars: Kepler rotation law

Next we see the results for the rotation law in Sec.2.5.3. We call the law as Kepler rotation. A contour plot of a nearly mass-shedding stellar model with Kepler rotation law is given in Fig.11. The core is rotationally deformed in a hamburger shape, on top of which a torus-like envelope resides. The pressure contour is highly elongated in the equatorial plane due to strong centrifugal force from the differential rotation. Compared with a nearly mass-shedding case of Yoon07 (Fig.8) the envelope is expanded more in the Kepler rotation law model.

We plot the mass-radius relation for $T_b = 5 \times 10^8 \text{ K}$ and $(X_C, X_O) = (0.2, 0.8)$ in Fig.12. The vertical dashed line corresponds to twice the Chandrasekhar mass of a cold non-rotating white dwarf. Beyond the line a sequence may lose

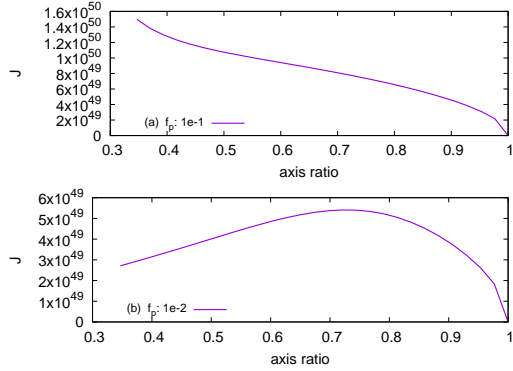


Figure 10. Angular momentum as a function of axis ratio. We fix $T_b = 5 \times 10^8 \text{ K}$, $\rho_c = 10^9 \text{ g cm}^{-3}$, and $(X_C, X_O) = (0.2, 0.8)$. The angular momentum is unit of $\text{g cm}^2 \text{ s}^{-1}$. The top panel (a) is for $f_p = 10^{-1}$, while the bottom one (b) is for $f_p = 10^{-2}$. For non-rotating stars the axis ratio is unity.

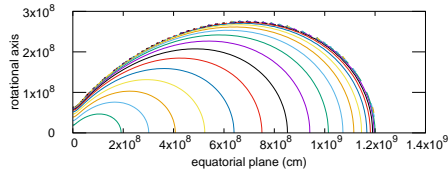


Figure 11. Pressure contour of a star close to its mass-shedding limit for Kepler rotation law. Thirty levels surfaces are equally spaced in logarithm of pressure. Assuming the axial and equatorial symmetry, we only plot a quadrant of the meridional cross section. The central density is 10^8 g cm^{-3} , pressure at the core-envelope boundary is $f_p = 10^{-1}$ and temperature at the boundary is $T_b = 5 \times 10^8 \text{ K}$. The total mass of the star is $3.15 M_\odot$, while the core mass is $1.56 M_\odot$. The equatorial core radius is $3.33 \times 10^8 \text{ cm}$. Dimensionless parameter T/W is 2.11×10^{-1} and the rotational angular frequency $\Omega = 0.488 \text{ Hz}$ at its equatorial surface.

its meaning for a model of a merger remnant. Numerical computations of sequences without asterisk are stopped at axis ratio equals 0.2. The sequence may be extended beyond this point and the stellar structure may take a "doughnuts" shape with off-center density maximum. Since our current code does not converge for very small axis ratio case, we stop the computation there. The mass and the T/W parameter may become also larger for the Kepler law. It should be noted that the core mass is also higher for the Kepler case as is seen in Fig.13. For given composition, T_b and ρ_c , the model with Kepler rotation has much higher mass for a given core mass ratio, which means both core and total

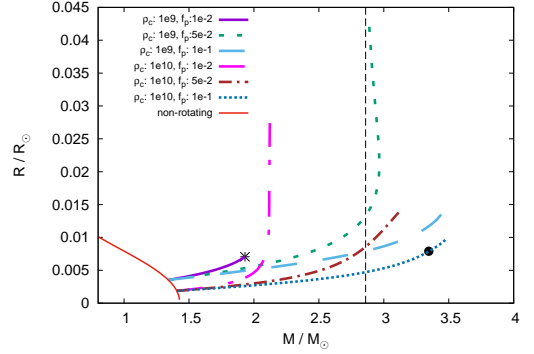


Figure 12. Mass-radius relation for the "Kepler." rotation law. All the models have $T_b = 5 \times 10^8 \text{ K}$ and $(X_C, X_O) = (0.2, 0.8)$. The filled circle marks the point above which the envelope mass exceeds that of the core, while the asterisk marks the mass-shedding limit. The dashed line corresponds to the mass twice as large as the Chandrasekhar mass of the non-rotating model for this composition ($M = 1.43 M_\odot$).

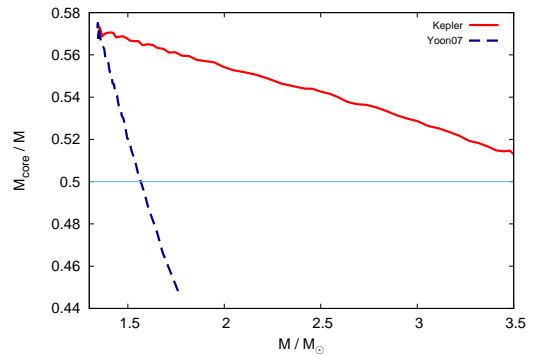


Figure 13. Ratio of the core mass to the total mass for Yoon07 and Kepler rotation laws. At the top-left point the model is non-rotating and the axis ratio is decreased to have models with larger degree of rotation along the sequence. Other parameters are fixed as $\rho_c = 10^9 \text{ g cm}^{-3}$, $T_b = 5 \times 10^8 \text{ K}$, $f_p = 10^{-1}$ and $(X_C, X_O) = (0.2, 0.8)$.

mass is much higher for Kepler rotation models. This is because the Yoon07 profile has a slowly rotating core while the Kepler has a rapidly rotating one. The centrifugal support against the self-gravity is larger for the latter case, which enables the larger core mass.

4 SOME EQUILIBRIUM SEQUENCES OF SIMPLIFIED EVOLUTION

As for evolutions and final fates of merger remnants of white dwarf binaries, there have been theoretical studies focusing on different phases of the remnant evolutions. Three-dimensional numerical hydrodynamic codes developed by different research groups have been used to follow successive phases of binary-inspirals, mergers and formation of remnants (Guillochon et al. 2010; Dan et al. 2011, 2012, 2014; Tanikawa et al. 2015; Sato et al. 2015, 2016). These studies mainly investigate the possibility of explosive carbon burning that leads to prompt explosion scenario of type Ia supernovae. Dan et al. (2014) and Sato et al. (2015) systematically surveyed the parameter space of possible progenitors of the supernovae. The other studies (Yoon et al. 2007; Schwab et al. 2012; Shen et al. 2012) have focused on evolutions of remnants in much longer time scale. In these studies outcomes of three-dimensional hydrodynamical simulations are projected onto one-dimensional codes that solve thermal, chemical and rotational evolution of a remnant in quasi-hydrostatic approximation. The secular evolution of remnants toward the so-called 'delayed explosion' is the main issue to be investigated. On the other hand Zhang et al. (2014) studied evolution of merger remnants as progenitors of R Coronae Borealis and extreme helium stars.

As an application of our new code, we construct equilibrium sequences that may mimic early evolutionary paths of merger remnants. Our motivation here is not to construct elaborated models of progenitors of supernovae or carbon rich subdwarfs. We study some characteristics of sequences and check viability of the rotating equilibria by a simple argument. Thus we do not go into a detailed study including thermal relaxation, nuclear reactions and radiative cooling, but study constrained sequences of equilibria with some global parameters being fixed. Particularly it should be noted that the temperature at the bottom of the envelope T_b may exceed 10^8K for some models below. In those cases helium burning may contribute to the heating of the envelope and the simple approximation here may not be adequate. The effect of the heating is beyond our scope here.

4.1 Sequences with fixed entropy in the envelope

First we fix specific entropy S_b of the hot envelope as well as the masses of the core and the entire star. The sequences are intended to mimic evolutions through rapid angular momentum loss compared with the thermal relaxation and dissipation. We do not specify the mechanism of angular momentum loss and assume the rotation law to be unchanged during an evolution. The sequences here are computed by iteratively solving for ρ_c , f_p , and the axis ratio with the total mass M , the core mass M_{core} , and the specific entropy of the envelope S_b being fixed.

In Fig.4.1 total energy E_{total} of stars is plotted as a function of angular momentum J . The total energy is defined as

$$E_{\text{total}} = \frac{1}{2} \int \rho \Phi dV + \frac{1}{2} \int \rho (\Omega r \sin \theta)^2 dV + \int \rho u dV, \quad (25)$$

where u is specific internal energy. Each term corresponds to gravitational, kinetic and thermal energy, respectively. The sequences have total mass $M = 1.16M_{\odot}$ and the core mass

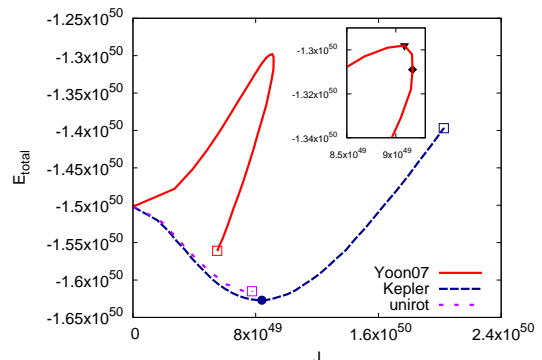


Figure 14. Sequences of equilibrium models on which the total mass $M = 1.16M_{\odot}$, the core mass $M_{\text{core}} = 0.84M_{\odot}$ and the specific entropy $S_b = 1.93 \times 10^8$ ($\text{erg g}^{-1}\text{K}^{-1}$) are fixed. The entropy value corresponds to $T_b = 1 \times 10^8$ (K) for the non-rotating model. Total energy of a star E_{total} (in ergs) is plotted against the total angular momentum J (in $\text{g cm}^2\text{s}^{-1}$). The open squares mark the mass-shedding limits of the sequence. The local minima of E_{total} are marked by the filled circles. The key "unirot" means the sequence with the uniform rotation. An enlargement of the part of Yoon07 sequence is shown in the inset. The filled diamond corresponds to the maximum of J , while the filled triangle corresponds to the maximum of E_{total} . The composition of the envelope is $X_{\text{He}} = 1$.

$M_{\text{core}} = 0.84M_{\odot}$. As for the composition of the envelope, we follow the scheme in Marsh (2011), whose Fig.1 shows the possible combinations of white dwarf's composition in the parameter space of the binary component's masses. For Fig., the lighter component of the progenitor ($M = 0.32M_{\odot}$) consists of pure helium ($X_{\text{He}} = 1$) for simplicity. We do not consider nuclear reactions to change the composition further.

On these sequences physically allowed segments are the ones on which total energy decreases as the total angular momentum decreases. Thus the natural branch that models an evolutionary path of a star should satisfy,

$$\left. \frac{dE_{\text{total}}}{dJ} \right|_{S_{\text{envelope}}} > 0, \quad (26)$$

where S_{envelope} is the total entropy of the envelope. For the current isentropic envelope $S_{\text{envelope}} = M_{\text{envelope}}S_b$. For the Kepler sequence, the total energy has a minimum marked by the filled circle. The segment on the right of the minima are the allowed ones if a star is not spun up by some external torque (e.g. due to accretion of fall back debris). Notice that the open squares mark the mass-shedding limit. A rapidly rotating star may evolve along the segment by losing their angular momentum and energy until they hit the minimum of E_{total} . After that the star may not evolve along the adiabatic sequence. On the other hand the uniform rotation sequence (whose key is "unirot") has no extremum, but terminates at the mass-shedding. Thus the uniformly rotating star with the parameter set may not be a model of the adiabatic spin-down evolution. Another curious feature is that the uniformly rotating sequence and the Kepler sequence are on top of each other. Similar behaviour is seen in the figures

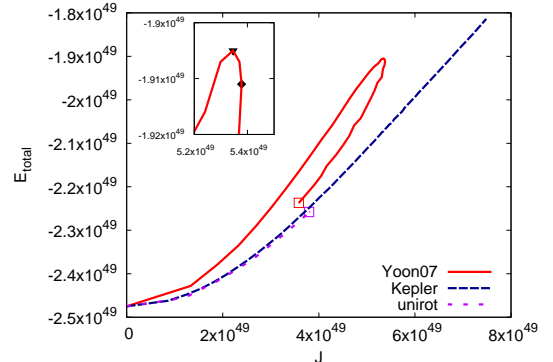
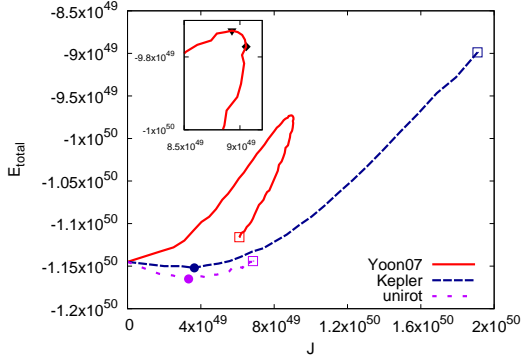


Figure 15. Same as Fig.4.1 except the total mass $M = 1.0M_{\odot}$, the core mass $M_{\text{core}} = 0.7M_{\odot}$ and the specific entropy $S_b = 3.11 \times 10^8$ (erg g $^{-1}$ K $^{-1}$) are fixed. The entropy value corresponds to $T_b = 5 \times 10^8$ (K) for the non-rotating model. Total energy of a star E_{total} (in ergs) is plotted against the total angular momentum J (in gcm 2 s $^{-1}$). The open squares mark the mass-shedding limits of the sequence. The local minima of E_{total} are marked by the filled circles. An enlargement of the part of Yoon07 sequence is shown in the inset. The filled diamond corresponds to the maximum of J , while the filled triangle corresponds to the maximum of E_{total} . The composition of the envelope is $X_{\text{He}} = 1$.

Figure 16. Same as Fig.4.1 except that the total mass $M = 0.5M_{\odot}$, the core mass $M_{\text{core}} = 0.3M_{\odot}$ and the specific entropy $S_b = 2.82 \times 10^8$ (erg g $^{-1}$ K $^{-1}$) are fixed. The entropy value corresponds to $T_b = 1 \times 10^8$ (K) for the non-rotating model. Total energy of a star E_{total} (in ergs) is plotted against the total angular momentum J (in gcm 2 s $^{-1}$). The open squares mark the mass-shedding limits of the sequence. These models are regarded as remnants of He+He white dwarf binaries. The composition of the envelope is $X_{\text{He}} = 1$.

that follow (Fig.15 - Fig.20). A Kepler model has a uniformly rotating core which has a dominant contribution to angular momentum when the total angular momentum is as small as that of mass-shedding model of uniformly rotating star. On the other hand the total energy is dominated by the gravitational binding energy which is mainly controlled by the massive core. As a result the uniformly rotating sequence and the Kepler sequence are close to each other. Beyond the angular momentum of the mass-shedding limit of the uniformly rotating sequence, the contribution from the differentially rotating envelope is no longer neglected on the Kepler sequences.

For Yoon07 rotation law, the situation is completely different. The sequence has two allowed segments. As is seen in the inset, the sequence has a maxima of total energy (marked by a filled triangle) and a maxima of angular momentum (marked by a filled diamond). The upper of the allowed segments starts from the maxima of E_{total} and terminates at the non-rotating star. The dimensionless rotational parameter T/W spans $0 \leq T/W \leq 0.068$. The lower segment starts from the maxima of J and terminates at the mass-shedding limit. Along it T/W decreases from 0.068 to 0.024 (at the mass-shedding). The latter segment is a non-trivial one appearing as a manifestation of high degree of differential rotation.

For higher entropy (temperature) of the envelope the uniformly rotating sequence may have a minimum of E_{total} . In Fig.15 we plot model sequences with the higher entropy for the similar mass as in Fig.4.1. The composition of the envelope is the same. Now the uniformly rotating sequence has a minima of E_{total} and there is a short segment from the mass-shedding limit (open square) to the minimum which

satisfies Eq.(26). We see the qualitatively similar behaviour for Yoon07 and Kepler sequences as in Fig.4.1.

In Fig.16 we see sequences of less massive remnants with $M = 0.5M_{\odot}$ and $M_{\text{core}} = 0.3M_{\odot}$. The composition of the envelope is $X_{\text{He}} = 1$, thus the sequence may be regarded as remnants of He+He white dwarf binaries. Qualitative behaviour of the sequence for Yoon07 is similar to that in Fig.4.1. As for Kepler and uniform rotation sequences, there are no minima on the sequence thus the model stars may spin down to non-rotating limit if the angular momentum loss takes place sufficiently fast. Notice that the rightmost point of the Kepler sequence is not a mass-shedding limit. It is the point beyond which our code gives no convergence, thus we terminated to construct a model.

In Fig.17 we see sequences of remnants with more massive envelope, for which $M = 1.26M_{\odot}$ and $M_{\text{core}} = 0.72M_{\odot}$. As we have envelope of $M_{\text{envelope}} = 0.54M_{\odot}$, we choose the composition of it as carbon and oxygen (Marsh 2011) and assume $X_{\text{C}} = 0.6$ and $X_{\text{O}} = 0.4$. Thus the sequence is regarded as remnants of CO+CO white dwarf binaries. Qualitative behaviour of the sequence for Yoon07 is similar to that in Fig.4.1. It has two definite segments corresponding to different rapid spin-down paths. As for uniform rotation sequence, the minimum of E_{total} is at the mass-shedding, thus the sequence is not regarded as a rapid spin-down evolution as in Fig.4.1. The Kepler sequence has a minimum of E_{total} , the right segment of which is regarded as a rapid spin-down path of evolution. Notice that the rightmost point of the Kepler sequence is not a mass-shedding limit but merely the point beyond which our code gives no convergence.

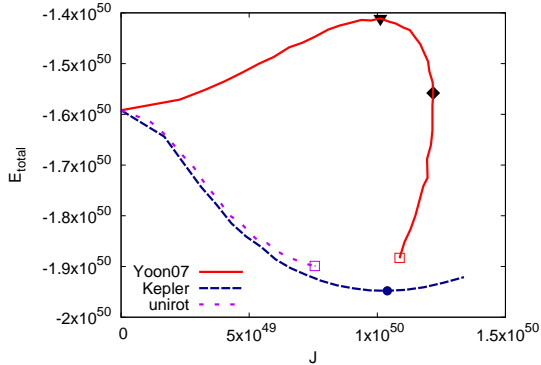


Figure 17. Same as Fig.4.1 except that the total mass $M = 1.26M_{\odot}$, the core mass $M_{\text{core}} = 0.72M_{\odot}$ with the envelope composition of $X_{\text{C}} = 0.6$, $X_{\text{O}} = 0.4$. The specific entropy $S_{\text{b}} = 6.16 \times 10^7$ ($\text{erg g}^{-1}\text{K}^{-1}$) are fixed. The entropy value corresponds to $T_{\text{b}} = 1 \times 10^8$ (K) for the non-rotating model. Total energy of a star E_{total} (in ergs) is plotted against the total angular momentum J (in $\text{gcm}^2\text{s}^{-1}$). The open squares mark the mass-shedding limits of the sequence. The filled diamond corresponds to the maximum of J , while the filled triangle corresponds to the maximum of E_{total} . These models are regarded as remnants of CO+CO white dwarf binaries.

4.2 Sequences with fixed angular momentum

We construct sequences by fixing angular momentum and total mass of stars as well their core mass. These sequences are intended to mimic the case when radiative cooling of the envelope is so efficient that stars do not spin down during the evolution. The sequences here are computed by iteratively solving for ρ_{c} , T_{b} , and the axis ratio, with the total mass M , the core mass M_{core} , and the total angular momentum J being constrained. On these sequence a natural evolutionary path is their segments on which the total energy E_{total} decreases as the entropy of their envelope decreases,

$$\left. \frac{dE_{\text{total}}}{dS_{\text{b}}} \right|_J > 0, \quad (27)$$

When the condition is satisfied, a star cools down along the sequence by conserving angular momentum until it hits a minimum of E_{total} . After that the angular momentum loss needs to be taken into account to consider the evolutionary path of the remnant.

In Fig.18 we plot E_{total} as functions of S_{b} for different rotation laws. Here the total mass and the core mass is fixed as $M = 1.0M_{\odot}$ and $M_{\text{core}} = 0.7$. The envelope composition is fixed as $X_{\text{He}} = 1$. We fix the angular momentum of all the sequences to be $J = 7.1 \times 10^{49} \text{gcm}^2\text{s}^{-1}$, which is the angular momentum of the uniformly rotating model at its mass-shedding limit (open square) for $T_{\text{b}} = 2.7 \times 10^8 \text{K}$.³ The uniformly rotating sequence and the Kepler sequence

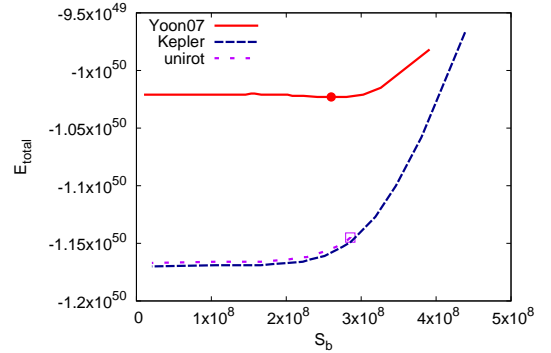


Figure 18. Sequences of equilibrium models on which the total mass the total mass $M = 1.0M_{\odot}$, the core mass $M_{\text{core}} = 0.7M_{\odot}$ and the angular momentum $J = 7.1 \times 10^{49} \text{gcm}^2\text{s}^{-1}$ are fixed. The horizontal axis is the specific entropy of the envelope S_{b} in $\text{erg g}^{-1}\text{K}^{-1}$. The vertical axis is the total energy of stars E_{total} in ergs. The open square marks the mass-shedding limits of the sequence. The local minimum of E_{total} is marked by the filled circle. The mass-shedding model for the uniform rotation law has $T_{\text{b}} = 2.7 \times 10^8 \text{K}$, while the leftmost points of the Yoon07 and Kepler sequences have $T_{\text{b}} = 7 \times 10^8 \text{K}$. The mass-shedding model for the sequence with uniform rotation law has $T_{\text{b}} = 2.7 \times 10^8 \text{K}$ while the left most point, of it has $T_{\text{b}} = 1 \times 10^6 \text{K}$. The composition of the envelope is $X_{\text{He}} = 1$.

with the same angular momentum satisfies Eq.(27) in the entropy range shown here. Thus a remnant formed on these sequence may cool all the way down to $T_{\text{b}} \sim 10^6 \text{K}$. Yoon07 sequence, on the other hand, have a minimum. Thus the evolutionary sequence of rapid cooling is terminated there ($T_{\text{b}} \sim 1.5 \times 10^8 \text{K}$).

In Fig.19 we plot sequences of fixed angular momentum for less massive remnants with $M = 0.5M_{\odot}$ and $M_{\text{core}} = 0.3M_{\odot}$. The fixed angular momentum is that of the mass-shedding limit star for uniform rotation and $T_{\text{b}} = 1.6 \times 10^8 \text{K}$. The sequences here satisfy Eq.(27) and it may be regarded as a rapid cooling evolutionary paths. Notice that the leftmost and rightmost points of the Yoon07 and the Kepler sequences are points at which our code do not give convergence.

For more massive remnant of CO+CO white dwarf mergers, the rapid cooling path may be marginally realized. In Fig.20 we plot the models with $M = 1.26M_{\odot}$ and $M_{\text{core}} = 0.72M_{\odot}$ whose envelope composition is $X_{\text{C}} = 0.6$, $X_{\text{O}} = 0.4$. The Yoon07 sequence does not satisfies Eq.(27). The uniform rotation and the Kepler sequences satisfies it down to $S_{\text{b}} \sim 10^8 \text{erg g}^{-1}\text{K}^{-1}$, below which the left hand side of Eq.(27) is nearly zero. The temperature range of the figure is roughly $T_{\text{b}} = 5 \times 10^7 \text{K}$ to $3 \times 10^8 \text{K}$, outside of which our code do not convergence.

³ Notice that this may underestimate the angular momentum of remnants which are supposed to be differentially rotating. More realistic value of angular momentum may be several factors or

an order of magnitude larger, thus it may be of the order of $10^{50} \text{gcm}^2\text{s}^{-1}$ (Gourgouliatos & Jeffery 2006).

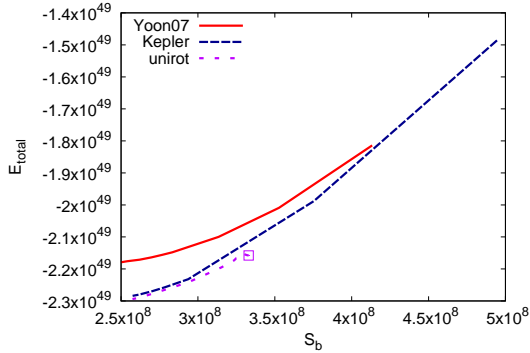


Figure 19. Same as Fig.18 except that $M = 0.5M_{\odot}$, the core mass $M_{\text{core}} = 0.3M_{\odot}$ and the angular momentum $J = 3.5 \times 10^{49} \text{ g cm}^2 \text{ s}^{-1}$ are fixed. The horizontal axis is the specific entropy of the envelope S_b in $\text{erg g}^{-1} \text{ K}^{-1}$. The vertical axis is the total energy of stars E_{total} in ergs. The open square marks the mass-shedding limits of the sequence. The local minimum of E_{total} is marked by the filled circle. The mass-shedding model for the uniform rotation law has $T_b = 1.6 \times 10^8 \text{ K}$ while the leftmost point of it has $T_b = 5.5 \times 10^7 \text{ K}$. For the Yoon07 sequence, temperature of the envelope at the rightmost and the leftmost points are $2.5 \times 10^8 \text{ K}$ and $5 \times 10^7 \text{ K}$ respectively. For the Kepler sequence, they are $2.5 \times 10^8 \text{ K}$ and $5.5 \times 10^7 \text{ K}$.

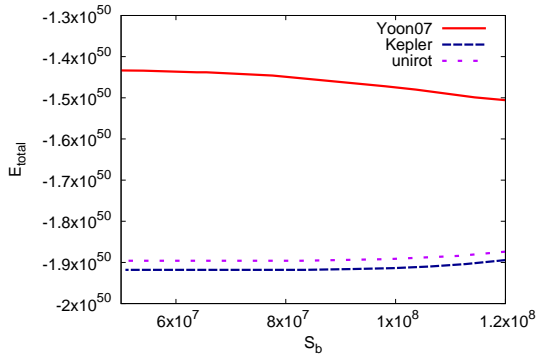


Figure 20. Same as Fig.18 except that the total mass $M = 1.26M_{\odot}$, the core mass $M_{\text{core}} = 0.72M_{\odot}$ and the angular momentum $J = 7.1 \times 10^{49} \text{ g cm}^2 \text{ s}^{-1}$ are fixed. The composition of the envelope is $(X_C, X_O) = (0.6, 0.4)$. For the uniformly rotating sequence, the rightmost and the leftmost points have $T_b = 8 \times 10^8 \text{ K}$ and $7 \times 10^6 \text{ K}$. For Yoon07 sequence, the temperature at the rightmost and the leftmost points are $9 \times 10^8 \text{ K}$ and $4 \times 10^7 \text{ K}$ respectively. For the Kepler sequence, they are $8 \times 10^8 \text{ K}$ and $3 \times 10^7 \text{ K}$.

5 SUMMARY

We present a new formalism to compute equilibrium of rotating star whose structure consists of two layers of thermal characteristics. The equation of state of the dense core is that of completely degenerate electrons, while the equation of state of the hot envelope is the tabulated ‘Helmholtz’ equation of state of Timmes & Swesty (2000). Our model is meant to mimic remnant objects of binary white dwarf mergers driven by gravitational radiation. In the final phase of in-spiraling the secondary star in a binary fills its Roche lobe and dynamically accreted onto the primary. The accreted matter is heated up to form a hot envelope, while the primary white dwarf stays in degenerate state as long as the thermal relaxation is negligible.

Given an angular frequency profile (rotation law), our model is parametrized by the composition of its core and envelope, the central density ρ_c , the temperature at the core-envelope boundary T_b , and the ratio of pressure at the core-envelope boundary to the central pressure f_p .

When its central density of the core is large enough, a model is close to completely degenerate star. The effect of hot envelope becomes significant when the central density and the core mass decreases. In this case, thermal pressure of hot envelope supports its mass against the gravity of the core and itself. The mass-radius relation depends on the chemical composition of the envelope, especially that of hydrogen. More hydrogen leads to reduction of the mean molecular weight of the envelope gas, resulting in the increase of thermal pressure for given temperature. As a result, the mass and radius are larger compared to the models lacking hydrogen in the envelope. It should be remarked, however, a model whose mass in the envelope exceeds that of the core may not be astrophysically relevant at least as a model of a merger remnant of a white dwarf binary. This is because the hot envelope originates from the secondary star of the binary. Non-rotating model would not produce super-Chandrasekhar object even with the presence of hot envelope.

Next we examine the effect of rotation on our models. Uniform rotation increases the mass and radius of the model by at most a few per cent even in the mass-shedding limit.

Introduction of differential rotation changes the picture drastically. We consider two rotational angular velocity profiles which are motivated by the preceding studies of merger remnants. One of these profiles has a slowly rotating core with a rapidly rotating envelope (“Yoon07”) while the other has a rapidly and uniformly rotating core with a Kepler-like distribution in the envelope (“Kepler”). In both cases the increment of mass and radius are more than the uniformly rotating counterparts. Especially in the Kepler case, highly super-Chandrasekhar models are possible whose mass doubles the Chandrasekhar mass of the non-rotating star, without encountering the dominance of envelope mass.

Another traits of differentially rotating sequences are the importance of f_p parameter. f_p is the parameter which determines where the core is truncated and the envelope is attached. Larger f_p means the bottom of the envelope have larger pressure, which makes the larger mass of the envelope possible. As a consequence, a larger f_p model has a larger total mass. This is not apparent in the uniformly rotating cases, where mass-shedding limit is reached before the effect

of f_p becomes important. For differentially rotating stars, the mass-radius relation is strongly affected by f_p .

As applications to the early phase of the evolution of the merger remnants, we consider sequences with total mass and the core mass (therefore the envelope mass as well) being fixed. When we fix the specific entropy of the envelope S_b , we may reduce the total angular momentum of the stars to construct the rapidly spinning-down sequences. As the angular momentum decreases, the total energy should not increase if the sequence is regarded as an evolutionary path. We see the sequences of uniform rotation and of Kepler rotation law are similar although the latter is extended to much larger value of angular momentum due to the strong differential rotation. For a massive remnant with $M \sim 1M_\odot$ and with helium envelope, both of the sequences have minima of total energy when the entropy is large enough (Fig.15). Thus a rapid spin-down evolution of these models are possible down to a finite value of angular momentum. Beyond that the thermal relaxation should not be neglected. For a smaller entropy envelope, however, the uniformly rotating star do not have an energy minimum (see Fig.4.1) and the sequence may not be regarded as that of the rapid spin-down. For a less massive sequence with $M = 0.5M_\odot$, the minima of the energy is at the non-rotating model. Thus the evolutionary path of rapid spin-down extends down to the non-rotating limit. For a massive remnant with carbon+oxygen envelope, the spin-down path is much shorter for the Kepler law and there is no spin-down path for the uniform rotation.

On the other hand, Yoon07 rotation law produces distinct sequences. We have two branches of evolutionary paths of rapid spin-down. One is a path connecting the non-rotating limit to the energy maximum. Another is a sequence starting from the maximum of angular momentum to the mass-shedding limit. The fate of a remnant at the end of its rapid spin-down era is thus completely different depending on which branch it is on. For the former path, the remnant may lose all the angular momentum (though we have not specified the mechanism of angular momentum loss). For the latter case, the remnant may shed its mass at the equator at the end of spin-down.

We also consider the sequence on which the total angular momentum is conserved, while the specific entropy decreases. This is meant to mimic the rapid cooling and slow spin-down evolution. A branch of the sequence on which total energy decreases as the entropy decreases is regarded as the evolutionary path. The uniform rotation and Kepler sequences are again similar though the latter sequence extend to larger value of entropy. They are monotonic in S_b thus the sequences are regarded as rapid cooling sequences. For the Yoon07 rotation law, the nature of the path strongly depends on the mass and the composition of the envelope. For a helium envelope case, the massive remnant has an energy minimum on the sequence (Fig.18) while the energy is monotonic for the less massive case (Fig.19). For the former case, a remnant born at a point on the right of the energy minimum rapidly cools down to the minimum. Beyond that the rapid cooling is no longer valid. For the latter case, the total energy is a decreasing function of the entropy. Thus the sequence is not regarded as an evolutionary path due to rapid cooling.

ACKNOWLEDGEMENTS

I thank the anonymous reviewer for his/her careful reading and suggestions that help to improve the paper. This work was supported by JSPS Grant-in-Aid for Scientific Research(C) 18K03641.

REFERENCES

- Balbus S. A., Hawley J. F., 1991, *ApJ*, 376, 214
Benz W., Bowers R. L., Cameron A. G. W., Press W. H. , 1990, *ApJ*, 348, 647
Boshkayev K., Quevedo H., 2018, *MNRAS*, 478, 1893
Boshkayev K., Rueda J., Ruffini R., 2011, *International Journal of Modern Physics E*, 20, 136
Boshkayev K., Rueda J. A., Ruffini R., Siutsou I., 2014, *Journal of Korean Physical Society*, 65, 855
Carvalho G. A., Marinho R. M., Malheiro M., 2018, *General Relativity and Gravitation*, 50, 38
Clayton G. C., Geballe T. R., Herwig F., Fryer C., Asplund M., 2007, *ApJ*, 662, 1220
Dan M., Rosswog S., Guillochon J., Ramirez-Ruiz E., 2011, *ApJ*, 737, 89
Dan M., Rosswog S., Guillochon J., Ramirez-Ruiz E., 2012, *MNRAS*, 422, 2417
Dan M., Rosswog S., Brügger M., Podsiadlowski P., 2014, *MNRAS*, 438, 14
Eriguchi Y., Müller E., 1985, *A&A*, 146, 260
Evans C. R., Iben Jr. I., Smarr L., 1987, *ApJ*, 323, 129
Fujisawa K., 2015, *MNRAS*, 454, 3060
García-Berro E., et al., 2012, *ApJ*, 749, 25
Gasques L. R., Afanasjev A. V., Aguilera E. F., Beard M., Chamon L. C., Ring P., Wiescher M., Yakovlev D. G., 2005, *Phys. Rev. C*, 72, 025806
Gourgouliatis K. N., Jeffery C. S., 2006, *MNRAS*, 371, 1381
Guillochon J., Dan M., Ramirez-Ruiz E., Rosswog S., 2010, *ApJ*, 709, L64
Hachisu I., 1986a, *ApJS*, 61, 479
Hachisu I., 1986b, *ApJS*, 61, 479
Hachisu I., 1986c, *ApJS*, 62, 461
Hayashi A., Eriguchi Y., Hashimoto M.-a., 1998, *ApJ*, 492, 286
Iben Jr. I., Tutukov A. V., 1984, *ApJS*, 54, 335
Izzard R. G., Jeffery C. S., Lattanzio J., 2007, *A&A*, 470, 661
Kadam K., Motl P. M., Frank J., Clayton G. C., Marcello D. C., 2016, *MNRAS*, 462, 2237
Kalogera V., Narayan R., Spergel D. N., Taylor J. H., 2001, *ApJ*, 556, 340
Kashyap R., Fisher R., García-Berro E., Aznar-Siguán G., Ji S., Lorén-Aguilar P., 2017, *ApJ*, 840, 16
Kawamura S., et al., 2006, *Classical and Quantum Gravity*, 23, S125
Kilic M., Hambly N. C., Bergeron P., Genest-Beaulieu C., Rowell N., 2018, *MNRAS*,
Kippenhahn R., Weigert A., 1994, *Stellar Structure and Evolution*
Loeb A., Rasio F. A., 1994, *ApJ*, 432, 52
Longland R., Lorén-Aguilar P., José J., García-Berro E., Althaus L. G., Isern J., 2011, *ApJ*, 737, L34
Lorén-Aguilar P., Guerrero J., Isern J., Lobo J. A., García-Berro E., 2005, *MNRAS*, 356, 627
Lorén-Aguilar P., Isern J., García-Berro E., 2009, *A&A*, 500, 1193
Luo J., et al., 2016, *Classical and Quantum Gravity*, 33, 035010
Maoz D., Hallakoun N., Badenes C., 2018, *MNRAS*, 476, 2584
Marsh T. R., 2011, *Classical and Quantum Gravity*, 28, 094019
Mathew A., Nandy M. K., 2017, *Research in Astronomy and Astrophysics*, 17, 061
Miyaji S., Nomoto K., Yokoi K., Sugimoto D., 1980, *PASJ*, 32, 303

- Nelemans G., 2009, *Classical and Quantum Gravity*, 26, 094030
- Nomoto K., Kondo Y., 1991, *ApJ*, 367, L19
- Pakmor R., Kromer M., Taubenberger S., Sim S. A., Röpke F. K., Hillebrandt W., 2012, *ApJ*, 747, L10
- Raskin C., Scannapieco E., Fryer C., Rockefeller G., Timmes F. X., 2012, *ApJ*, 746, 62
- Rueda J. A., et al., 2018, arXiv e-prints,
- Saio H., Nomoto K., 1985, *A&A*, 150, L21
- Sato Y., Nakasato N., Tanikawa A., Nomoto K., Maeda K., Hachisu I., 2015, *ApJ*, 807, 105
- Sato Y., Nakasato N., Tanikawa A., Nomoto K., Maeda K., Hachisu I., 2016, *ApJ*, 821, 67
- Schwab J., Shen K. J., Quataert E., Dan M., Rosswog S., 2012, *MNRAS*, 427, 190
- Schwab J., Quataert E., Kasen D., 2016, *MNRAS*, 463, 3461
- Segretain L., Chabrier G., Mochkovitch R., 1997, *ApJ*, 481, 355
- Shapiro S. L., Teukolsky S. A., 1986, *Black Holes, White Dwarfs and Neutron Stars: The Physics of Compact Objects*
- Shen K. J., Bildsten L., Kasen D., Quataert E., 2012, *ApJ*, 748, 35
- Tanikawa A., Nakasato N., Sato Y., Nomoto K., Maeda K., Hachisu I., 2015, *ApJ*, 807, 40
- Tassoul J.-L., 1978, *Theory of rotating stars*, Chap.10. Princeton University Press, New Jersey
- Timmes F. X., Swesty F. D., 2000, *ApJS*, 126, 501
- Uryu K., Eriguchi Y., 1994, *MNRAS*, 269, 24
- Uryu K., Eriguchi Y., 1995, *MNRAS*, 277, 1411
- Webbink R. F., 1984, *ApJ*, 277, 355
- Wickramasinghe D. T., Ferrario L., 2000, *PASP*, 112, 873
- Yoon S.-C., Podsiadlowski P., Rosswog S., 2007, *MNRAS*, 380, 933
- Zhang X., Jeffery C. S., Chen X., Han Z., 2014, *MNRAS*, 445, 660
- Zhu C., Chang P., van Kerkwijk M. H., Wadsley J., 2013, *ApJ*, 767, 164

This paper has been typeset from a $\text{\TeX}/\text{\LaTeX}$ file prepared by the author.